Case Study 9

Detecting Phytoplankton Community Structure from Ocean Colour

R.J.W. Brewin[*1], **N.J. Hardman-Mountford**[2], **T. Hirata**[3]

9.1 Background

Phytoplankton play a fundamental role in the biogeochemical cycling of the planet, with different phytoplankton communities having specific biogeochemical roles (Le Quéré et al. 2005; Nair et al. 2008). Phytoplankton support marine ecosystems as the primary carbon source for zooplankton, fish and ultimately higher predators. Furthermore, zooplankton and fish can have selective feeding preferences for phytoplankton of different sizes and types (Hansen et al. 1994; Scharf et al. 2000; Jennings et al. 2002). By improving our understanding of the spatial structure of the different phytoplankton communities, advances in biogeochemical and food-web models can be made, which may enhance our comprehension of the Earth system needed to predict future change.

Methods that can identify and quantify different elements of the phytoplankton community can provide useful information to help understand biogeochemical and ecological processes. Observing the *in situ* size structure and taxonomic grouping of phytoplankton at a global scale is, however, a challenging task. Satellite observation is currently the only practical method of observing the global ocean synoptically. With increasing concern as to how climate variation is affecting marine ecosystems, there is a large expectation of satellite remote sensing to provide global observations of the taxonomic or functional groups of phytoplankton, moving beyond conventional pigment biomass (i.e. chlorophyll).

Recently, a variety of bio-optical and ecological methods have been established that use satellite data to identify and differentiate between phytoplankton functional types (PFTs) or phytoplankton size classes (PSCs) in the surface ocean. These can be summarised into four main types: spectral-response methods which are based on

[1]School of Marine Science and Engineering, University of Plymouth, UK. **Email address:* robert.brewin@plymouth.ac.uk
[2]National Centre for Earth Observation, Plymouth Marine Laboratory, UK
[3]Faculty of Environmental Earth Science, Hokkaido University, Japan

differences in the shape of the light reflectance/absorption spectrum for different PFTs/PSCs (Sathyendranath et al. 2004; Alvain et al. 2005; Ciotti and Bricaud 2006; Alvain et al. 2008; Brewin et al. 2010a), abundance-based methods which use information on the magnitude of chlorophyll biomass or light absorption to distinguish between phytoplankton communities (Devred et al. 2006; Uitz et al. 2006; Hirata et al. 2008a; Brewin et al. 2010b; Hirata et al. 2010), methods that retrieve the particle size distribution from satellite-derived backscattering signal and then relate the particle size to the phytoplankton community (Hirata et al. 2008b; Kostadinov et al. 2009), and ecological-based approaches which use information on environmental factors, such as temperature and wind stress to supplement the bio-optical data for investigating specific taxa (Raitsos et al. 2008). Recent intercomparison studies suggest that abundance-based approaches appear robust at detecting dominant phytoplankton size classes (Brewin et al. 2008).

9.1.1 Phytoplankton size class model

Here we present a method for determining the fractional contribution of a phytoplankton size class (pico- $<2\mu$m, nano- 2-20μm and micro-phytoplankton $>20\mu$m) to the overall chlorophyll concentration (Brewin et al. 2010b). The model is an extension of the Sathyendranath et al. (2001) approach, based on the assumption that small cells dominate at low chlorophyll concentrations and large cells at high concentrations. The model can be expressed through two simple exponential equations. In this example the subscripts 1, 2 and 3 refer to pico-, nano- and microphytoplankton, and the total chlorophyll-*a* concentration is referred to as C (mg m^{-3}). Firstly, the chlorophyll concentration of the combined pico-nanophytoplankton population ($C_{1,2}$) can be expressed as:

$$C_{1,2} = {C_{1,2}}^{m}[1 - \exp(-S_{1,2}C)], \tag{9.1}$$

where, ${C_{1,2}}^{m}$ is the asymptotic maximum value for $C_{1,2}$ and $S_{1,2}$ determines the increase in $C_{1,2}$ with increasing total chlorophyll (C). Secondly, the chlorophyll concentration of the picophytoplankton population (C_1) can be expressed as:

$$C_1 = {C_1}^{m}[1 - \exp(-S_1C)], \tag{9.2}$$

where ${C_1}^{m}$ is the asymptotic maximum value for C_1 and S_1 determines the increase in C_1 with increasing total chlorophyll-*a* (C). The chlorophyll-*a* concentration of nanophytoplankton (C_2) and microphytoplankton (C_3) can then be calculated according to:

$$C_2 = C_{1,2} - C_1, \tag{9.3}$$

$$C_3 = C - C_{1,2}. \tag{9.4}$$

The percentage of each phytoplankton size class to the total chlorophyll concentration (C) can then be calculated by dividing the size-specific chlorophyll concentrations (C_1, C_2 and C_3) by the total chlorophyll concentration (C) and multiplying by 100, such that

$$P_1 = (C_1/C) \times 100, \tag{9.5}$$

$$P_2 = (C_2/C) \times 100, \tag{9.6}$$

$$P_3 = (C_3/C) \times 100, \tag{9.7}$$

where P_1, P_2 and P_3 represent the percentages of pico-, nano- and microphytoplankton to the total chlorophyll concentration (C). Parameter values for ${C_{1,2}}^m$, ${C_1}^m$, $S_{1,2}$ and S_1 were taken from Table 1 in Brewin et al. (2010b), and set to 1.06, 0.11, 0.85 and 6.80, respectively. When using these parameters, the model performed well when applied to satellite chlorophyll data and compared with *in situ* measurements (see section 4.3 in Brewin et al. 2010b).

Figure 9.1 shows the results from applying the model of Brewin et al. (2010b) to SeaWiFS satellite data for January and July 2006. The model was applied to daily total chlorophyll (C) images from each month and then averaged to produce the two monthly composite images. The results show clearly that very small phytoplankton cells (picophytoplankton, $<2\mu$m) dominate in the low-production, subtropical gyres, medium-sized cells (nanophytoplankton, 2-20 μm) predominate in the equatorial upwelling area and in higher latitude regions depending on the boreal or austral summer. Relatively large cells (microphytoplankton, $>20\mu$m) dominate in coastal areas and during highly productive events, such as high-latitude spring/summer blooms. Furthermore, the size fractionation shows that nanophytoplankton tend to maintain a background population of between 20-50% of the standing stock in most regions, whereas pico- and microphytoplankton have larger spatial variability.

9.1.2 Equatorial Pacific

The equatorial Pacific is a unique region of our oceans. It can act as a large source of CO_2 to the atmosphere through the upwelling of CO_2-rich waters along the equator and advection of CO_2-rich waters from the South-American coast (Etcheto et al. 1999; Feely et al. 1999), and also a sink though primary production and export (Takahashi et al. 2002). It is one of only three open-ocean areas that, despite having high nitrate and phosphate concentrations, display moderately-low phytoplankton biomass (Martin 1991; Behrenfeld et al. 1996) and are referred to as exhibiting High Nutrient, Low Chlorophyll characteristics (HNLC, Thomas 1979). This enigma has been linked to either the lack of iron that limits the growth of the phytoplankton (Martin and Fitzwater 1988; Behrenfeld et al. 1996; Coale et al. 1996) or to a large amount

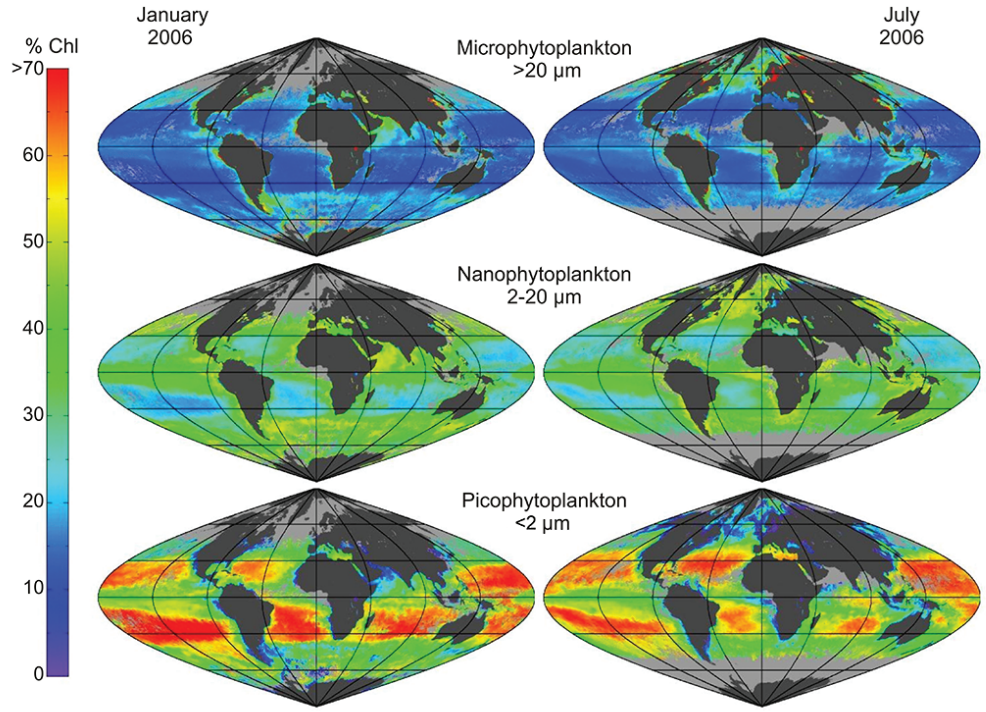

Figure 9.1 The percentage of total chlorophyll-*a* attributed to each of three phytoplankton size classes calculated according to the model of Brewin et al. (2010b), for the months of January and July 2006. The model was applied to daily Level 3 SeaWiFS composite images from each month and then averaged to produce monthly composites. Light grey pixels represent unidentified pixels due to cloud coverage or high sun zenith angles and dark grey pixels represent land.

of grazing from higher trophic levels that limits phytoplankton growth (Walsh 1976; Cullen 1991). Despite exhibiting moderately-low phytoplankton biomass, changes in the phytoplankton composition and sporadic large-scale accumulations of phytoplankton biomass have been found to occur (Chavez et al. 1990; Ryan et al. 2002), making the equatorial Pacific an ideal site to monitor variations in phytoplankton composition from satellite.

The model of Brewin et al. (2010b) was developed using an extensive dataset from the Atlantic Ocean, and validated using data with wider geographical coverage. However, the model of Brewin et al. (2010b) has not been validated in the equatorial Pacific. In light of this, 32 High Performance Liquid Chromatography (HPLC) pigment measurements (depth <10m) were downloaded from the NASA SeaBASS dataset (Werdell and Bailey 2002). Using diagnostic pigment analysis (Vidussi et al. 2001; Uitz et al. 2006; Brewin et al. 2010b) the *in situ* size-specific chlorophyll concentrations (C_1, C_2 and C_3) and size-specific percentage contributions to the total chlorophyll concentration (P_1, P_2 and P_3) were calculated for each sample. Then the

model of Brewin et al. (2010b) was applied to the *in situ* chlorophyll concentration to estimate C_1, C_2, C_3, P_1, P_2 and P_3 (Equations 9.1 – 9.7). Figure 9.2 shows the location of the 32 pigment measurements and a comparison between the diagnostic pigment-derived values and the values derived using the model. The two agreed well with an absolute root mean square error (RMSE) of 0.006 to 0.010 mg m^{-3} for the size-specific chlorophyll concentrations, and between 4.4 to 9.4 % for the percentage contributions to the total chlorophyll concentration, supporting the application of the Brewin et al. (2010b) model to the equatorial Pacific.

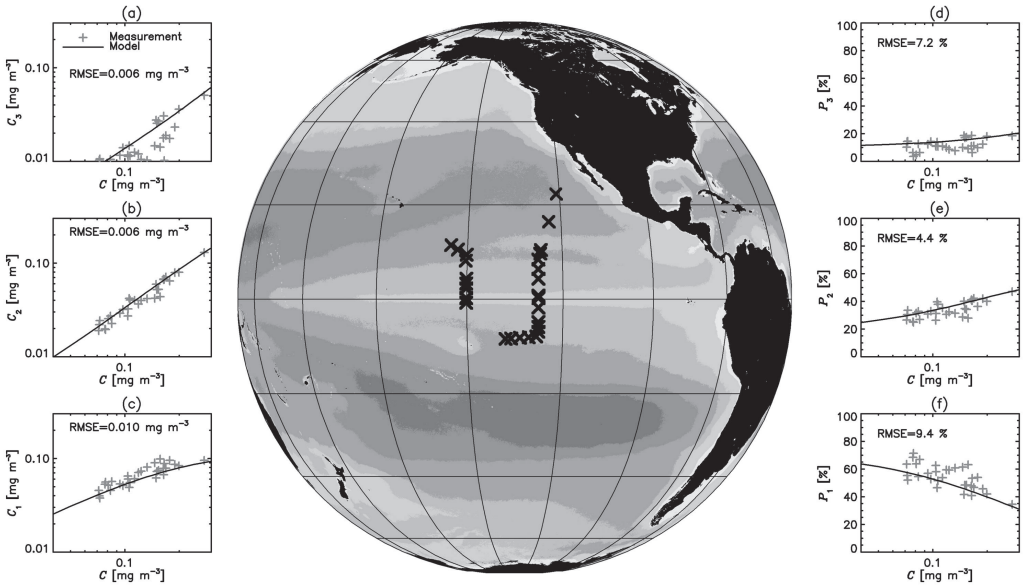

Figure 9.2 Location of the 32 HPLC pigment measurements used to validate the model of Brewin et al. (2010b) for use in the equatorial Pacific. The biome-based system of Hardman-Mountford et al. (2008) is superimposed on the globe with dark grey to light grey areas representing a transition from biomes with very low chlorophyll-*a* to biomes with very high chlorophyll-*a* . Results of the validation are shown to the left (C_1, C_2 and C_3) and right (P_1, P_2 and P_3) of the globe.

In this case study we apply the model of Brewin et al. (2010b) to daily, Level 3, SeaWiFS chlorophyll composites to produce two 8-day composites of the percentage contribution of the three size classes to total chlorophyll (P_1, P_2 and P_3), for 28 July – 4 August 1998 and 2003. We also produce two images of SST derived from the Advanced Very High Resolution Radiometer (AVHRR) sensor, for the same time periods. Differences in SST and the community composition of the three size classes, for the same seasonal week in the two contrasting years, are mapped in the equatorial Pacific.

9.2 Data and Methods

Sixteen daily Level 3 mapped SeaWiFS chlorophyll composites were downloaded from the NASA ocean colour website (http://oceancolor.gsfc.nasa.gov/), encompassing two eight-day periods.

- Week 1 (28 July – 4 August 1998)
- Week 2 (28 July – 4 August 2003)

All SeaWiFS data were extracted from the zipped format. Two SST AVHRR global composites for the same 8-day periods (week 1 and 2) were downloaded from the NASA Jet Propulsion Laboratory Physical Oceanography Distributed Active Archive Centre (ftp://podaac.jpl.nasa.gov/). Night time AVHRR Pathfinder (Version 5) 8-day means of sea surface temperature (SST) at 4 x 4 km^2 resolution were used. Night time SST products were used so that the solar radiation bias (the diurnal fluctuation in SST) that can occur from surface heating during daytime could be avoided. We used global, equal-angle, best SST. Information on the data used in this study is outlined in Table 9.1.

The software used in this study was IDL Version 6.3, Microsoft Windows (Win32 x86 m32). All IDL code developed for this study is available at http://www.ioccg.org/handbook/Brewin/. The procedure below has been developed into an IDL program (Handbook_RS_PSC_code.pro) to allow the reader to reproduce this example (see section 1.4 Training below).

The first step involves loading the sixteen daily Level 3 mapped SeaWiFS chl-*a* composites into the IDL program. All sixteen daily SeaWiFS composites are loaded into IDL using code developed by the Ocean Color Discipline Processing Group (readl3smi.pro). This code is designed to simplify the reading of SeaWiFS standard L3 mapped images, and converts the digital numbers (DN) of the image to chlorophyll-*a* values (mg m^{-3}). Once these images are loaded, the Brewin et al. (2010b) algorithm (Equations 9.1 – 9.7) is applied to each daily image on a pixel-by-pixel basis to derive P_1, P_2 and P_3 (the percentages of pico-, nano- and microphytoplankton to the total chlorophyll-*a* concentration (C)).

The daily composites from week 1 are then averaged to create 8-day composites of P_1, P_2 and P_3, and the same averaging is applied to the eight daily composites from week 2. Note that we applied the Brewin et al. (2010b) algorithm to daily images then averaged to produce an 8-day composite, as opposed to applying the algorithm directly to 8-day SeaWiFS chlorophyll-*a* composites, as the nonlinearity of equations 1 and 2 could introduce errors when applying the model directly to 8-day SeaWiFS chlorophyll-*a* composites.

The two SST images are then loaded into IDL using IDL code developed by the National Oceanographic Data Centre (pathfinder_v5_hdf_read.pro). Once these images are loaded, the data is converted to SST values (°C) from digital numbers (DN) according to:

$$\mathrm{SST} = 0.075 \times \mathrm{DN} - 3.0, \tag{9.8}$$

where the value 0.075 represents the slope and -3.0 the y-intercept. This results in six, 8-day, 9 x 9 km^2 resolution composites (arrays of [4320, 2160]) of P_1, P_2 , P_3 for both week 1 and 2, and two 8-day 4 x 4 km^2 resolution composites (arrays of [8192, 4096]) of SST for both week 1 and 2. The differences between the two contrasting weeks are then calculated according to:

$$P_{1,\mathrm{D}} = P_1(\mathrm{week1}) - P_1(\mathrm{week2}), \tag{9.9}$$

$$P_{2,\mathrm{D}} = P_2(\mathrm{week1}) - P_2(\mathrm{week2}), \tag{9.10}$$

$$P_{3,\mathrm{D}} = P_3(\mathrm{week1}) - P_3(\mathrm{week2}), \tag{9.11}$$

$$\mathrm{SST_D} = \mathrm{SST}(\mathrm{week1}) - \mathrm{SST}(\mathrm{week2}), \tag{9.12}$$

where, $P_{1,\mathrm{D}}$, $P_{2,\mathrm{D}}$, $P_{3,\mathrm{D}}$ and $\mathrm{SST_D}$ refer to the difference between the three size classes and SST of the two contrasting weeks. This results in 12 images to be used for analysis: P_1(week1), P_2(week1), P_3(week1), SST(week1), P_1(week2), P_2(week2), P_3(week2), SST(week2), $P_{1,\mathrm{D}}$, $P_{2,\mathrm{D}}$, $P_{3,\mathrm{D}}$ and SST_D. All 12 images are then rescaled to 36 x 36 km^2 resolution, to reduce computational requirements when plotting the images.

A plotting procedure is then set up to plot each of these 12 images and re-project them using an orthographic projection. The corresponding latitude and longitude values were calculated for each pixel. Values of each pixel in the image are binned into 256 ranges, and each range is assigned a colour depending on the colour scheme chosen. These 256 bins are then plotted onto an image of 1080 by 540 pixels, with each pixel representing 36 x 36 km^2 resolution. All pixels with no values (either due to cloud coverage or high sun zenith angles) are binned and assigned a light grey colour before being plotted. Using the SeaWiFS entire mission chlorophyll-*a* composite, a land mask has been developed (see "Land_mask", http://www.ioccg.org/handbook/Brewin/Data/) and the land is assigned a dark grey colour before being plotted onto the image.

Each image is then re-projected to an orthographic projection using the IDL functions "map_set.pro" and "map_proj_image.pro". Here we took the latitude of the point on the Earth's surface to be mapped to the centre of the projection plane to be 0°, and the longitude of the point on the Earth's surface to be mapped to the centre of the map projection to be -130°, to focus our attention to the equatorial Pacific. All 12 images are then projected onto the same image montage for analysis, and the respective colour bars for each image are also plotted (Figure 9.3).

Table 9.1 Satellite data used in the study (also available at http://www.ioccg.org/handbook/Brewin/Data/), including a land mask.

Date	Data	Filename	Location	Use
28/07/98	chl-a	S1998209.L3m_DAY _CHL_chlor_a_9km.bz2	http://oceancolor.gsfc.nasa.gov/cgi/l3	8-day PSC
29/07/98	chl-a	S1998210.L3m_DAY _CHL_chlor_a_9km.bz2	http://oceancolor.gsfc.nasa.gov/cgi/l3	8-day PSC
30/07/98	chl-a	S1998211.L3m_DAY _CHL_chlor_a_9km.bz2	http://oceancolor.gsfc.nasa.gov/cgi/l3	8-day PSC
31/07/98	chl-a	S1998212.L3m_DAY _CHL_chlor_a_9km.bz2	http://oceancolor.gsfc.nasa.gov/cgi/l3	8-day PSC
01/08/98	chl-a	S1998213.L3m_DAY _CHL_chlor_a_9km.bz2	http://oceancolor.gsfc.nasa.gov/cgi/l3	8-day PSC
02/08/98	chl-a	S1998214.L3m_DAY _CHL_chlor_a_9km.bz2	http://oceancolor.gsfc.nasa.gov/cgi/l3	8-day PSC
03/08/98	chl-a	S1998215.L3m_DAY _CHL_chlor_a_9km.bz2	http://oceancolor.gsfc.nasa.gov/cgi/l3	8-day PSC
04/08/98	chl-a	S1998216.L3m_DAY _CHL_chlor_a_9km.bz2	http://oceancolor.gsfc.nasa.gov/cgi/l3	8-day PSC
28/07/03	chl-a	S2003209.L3m_DAY _CHL_chlor_a_9km.bz2	http://oceancolor.gsfc.nasa.gov/cgi/l3	8-day PSC
29/07/03	chl-a	S2003210.L3m_DAY _CHL_chlor_a_9km.bz2	http://oceancolor.gsfc.nasa.gov/cgi/l3	8-day PSC
30/07/03	chl-a	S2003211.L3m_DAY _CHL_chlor_a_9km.bz2	http://oceancolor.gsfc.nasa.gov/cgi/l3	8-day PSC
31/07/03	chl-a	S2003212.L3m_DAY _CHL_chlor_a_9km.bz2	http://oceancolor.gsfc.nasa.gov/cgi/l3	8-day PSC
01/08/03	chl-a	S2003213.L3m_DAY _CHL_chlor_a_9km.bz2	http://oceancolor.gsfc.nasa.gov/cgi/l3	8-day PSC
02/08/03	chl-a	S2003214.L3m_DAY _CHL_chlor_a_9km.bz2	http://oceancolor.gsfc.nasa.gov/cgi/l3	8-day PSC
03/08/03	chl-a	S2003215.L3m_DAY _CHL_chlor_a_9km.bz2	http://oceancolor.gsfc.nasa.gov/cgi/l3	8-day PSC
04/08/03	chl-a	S2003216.L3m_DAY _CHL_chlor_a_9km.bz2	http://oceancolor.gsfc.nasa.gov/cgi/l3	8-day PSC
28/07/98 - 04/08/98	SST	1998209-1998216. s0481pfv50-bsst-16b	ftp://podaac.jpl.nasa.gov/pub/	8-day SST
28/07/03 - 04/08/03	SST	2003209-2003216. s0484pfv50-bsst	ftp://podaac.jpl.nasa.gov/pub/	8-day SST

9.3 Demonstration Section

Figure 9.3 shows a plot of the 12 images developed in the previous section where (a), (d), (g) and (j) are from week 1, (b), (e), (h) and (k) are from week 2, and (c), (f), (i), and (l) show the differences between the two weeks. The percentage of chlorophyll-*a* attributed to microphytoplankton is shown in the top three images (a-c), that attributed to nanophytoplankton in the next three (d-f), then picophytoplankton (g-i). The bottom three images represent SST (°C, j-l).

When analysing the microphytoplankton images (Figure 9.3a-c), one notices a higher proportion of microphytoplankton in the equatorial region during week 1 compared with week 2. This is highlighted in Figure 9.3c which shows the differences between the two microphytoplankton images and indicates 20% higher microphytoplankton % chlorophyll-*a* in the equatorial Pacific during week 1, with differences as high as 50% in the centre of this bloom, when compared with week 2.

When analysing the nanophytoplankton images (Figure 9.3d-f), one also notes slightly higher nanophytoplankton % chlorophyll-*a* in the equatorial region and slightly lower % chlorophyll-*a* just south-east of the equator during week 1 when compared with week 2 (Figure 9.3f). In contrast to the microphytoplankton, there is a significantly lower picophytoplankton % chlorophyll-*a* in the equatorial region during week 1 when compared with week 2 (Figure 9.3i). Furthermore, in contrast to nanophytoplankton, higher picophytoplankton % chlorophyll-*a* can be observed just south-east of the equator during week 1, compared with week 2 (Figure 9.3i).

Turning our attention to the SST images (Figure 9.3j-l), significant differences are noted between the two weeks. During week 1, lower SST values are seen in the central equatorial Pacific and slightly higher SST values in the south-east equatorial Pacific when compared with week 2.

9.4 Training

To help interpret the case study, we will now go through each of the steps to generate Figure 9.3. An IDL program (Handbook_RS_PSC_code.pro) was developed to allow the reader to reproduce this example.

- Step 1: Download all the files needed for the case study (Table 1) from `http://www.ioccg.org/handbook/Brewin/Data/` and save them to an appropriate folder on your desktop. Extract all the SeaWiFS files with the extension ".bz2" from their zipped format.
- Step 2: Download all the IDL code needed for the case study from `http://www.ioccg.org/handbook/Brewin/IDL%20Code/` and save it to your IDL path directory.
- Step 3: Open IDL and type `"handbook_RS_PSC_code"` into the command prompt. A dialog box will appear titled "Browse for folder". Locate the folder

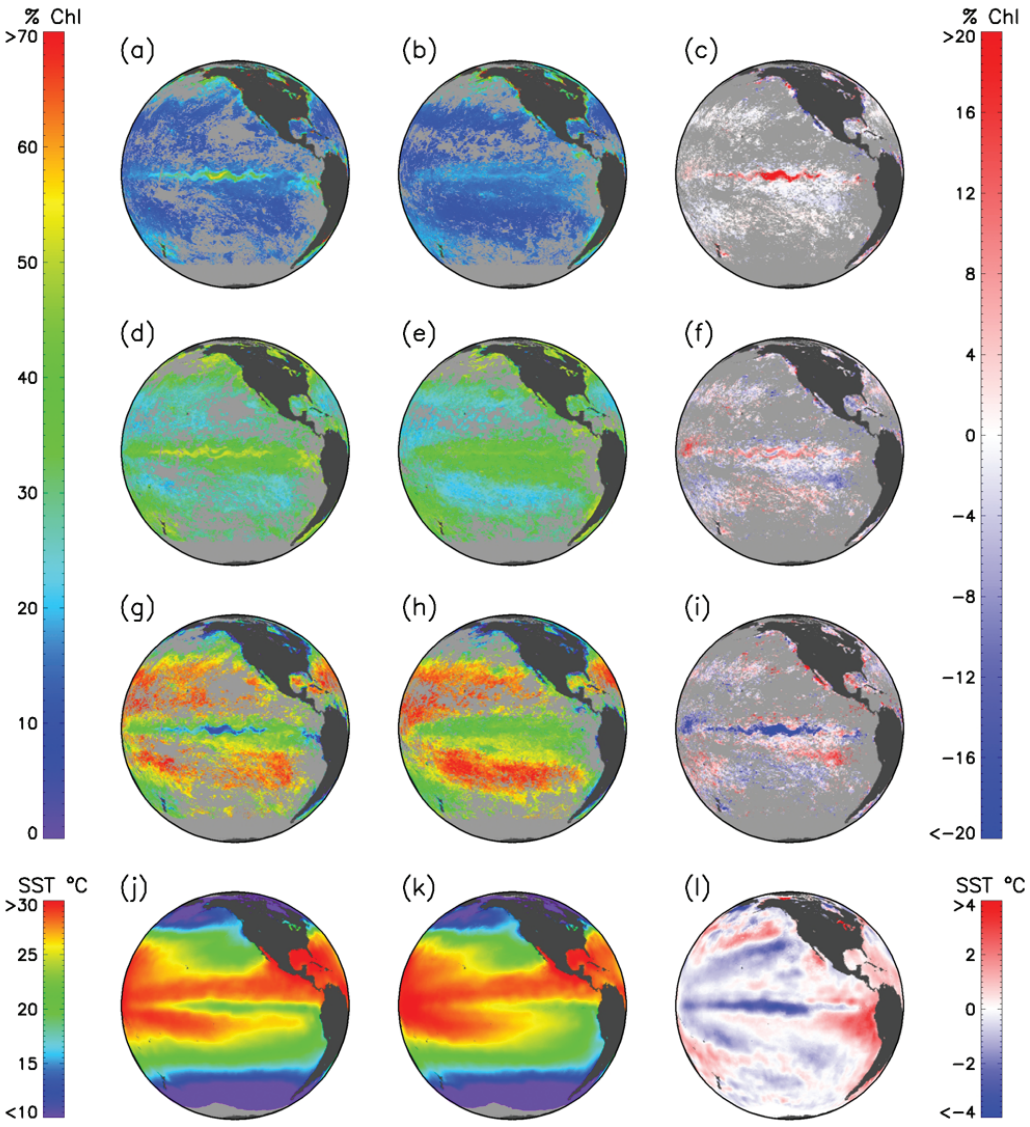

Figure 9.3 Plot of the 12 images developed in the case study. Figures (a), (d), (g) and (j) are from week 1, (b), (e), (h) and (k) from week 2, and (c), (f), (i), and (l) show the differences between the two weeks. Microphytoplankton % chlorophyll-*a* is shown in the top three images (a-c), followed by nanophytoplankton (d-f), then picophytoplankton (g-i), and at the bottom are the three SST images (j-l) in °C.

where you saved the input data in step 1 and press "OK".

- Step 4: The code will then run through the methodology described in section 9.2 (Data and Methods) and save Figure 9.3 to the directory where the files

were downloaded in step 1.

- ❖ NOTE: This program was run on Windows, using an Intel(R) Core(TM) 2 CPU 6320 @ 1.86GHz with 1.97GB of RAM. Using this computer, the code takes about 8 minutes to run. The code may take longer/shorter to run on other machines, may need to be manipulated for a UNIX/LINUX environment, and may need to be manipulated for other version of IDL (currently developed for IDL Version 6.3).

9.5 Questions

Q1: What phenomena may be causing the high microplankton % chlorophyll-*a* (Figure 9.3a) and the low SST values (Figure 9.3j) in the central equatorial Pacific during week 1?

Q2: Considering that the two 8-day composites are taken at the same seasonal time period, why are there such large differences in both SST and the phytoplankton community composition in Figure 9.3c, f, i and l?

Q3: How do the higher SST values south-east of the equatorial Pacific in week 1 (Figure 9.3j and l) appear to be influencing the phytoplankton community composition?

9.6 Answers

A1: The phenomena causing the high microplankton % chlorophyll-a (Figure 9.3a) and the low SST values (Figure 9.3j) in week 1, in the central equatorial Pacific, is the 1997-1999 El Niño/La Niña event. The periodic occurrence of El Niño and La Niña episodes has a strong effect on the physical forcing in the equatorial Pacific. Under non-El Niño conditions, easterly trade winds create a channel of cold surface water along the equator, referred to as the Eastern Equatorial Undercurrent (EUC). The EUC flows eastward across the equator at a depth of 20 to 200 m (Toggweiler and Carson 1995). During an El Niño event, a weakening or reversal of the trade winds occurs, which weakens the EUC and hence subdues the upwelling of cold nutrient rich waters and deepens the thermocline. Surface waters become warmer and nutrient poor. During a La Niña event, there is a strengthening of the trade winds, which strengthens the EUC, enhancing the upwelling of cold nutrient rich waters and raising the thermocline.

The 1997-1999 El Niño/La Niña event was the strongest of the 20th century (Kerr 1998; McPhaden 1999). During July/August 1998 (week 1) a large La Niña event occurred which strengthened the trade winds resulting in upwelling of cold nutrient rich waters close to the surface (McPhaden 1999). This is clearly seen in Figure 9.3l by the lower SST values during week 1 when compared with week 2 in the

central equatorial Pacific (note that week 2 was during a non- El Niño/La Niña year). This injection of cold nutrient rich waters during July/August 1998 ignited a huge surface phytoplankton bloom, with a 40-fold increase in chlorophyll-*a* (Chavez et al. 1999). This phytoplankton bloom is the largest phytoplankton bloom observed in the equatorial Pacific to date. This bloom, driven by the EUC, migrated from east to west at a speed of 105 km day^{-1} and its shape was distorted by Tropical Instability Waves (TIWs) (Chavez et al. 1999; Ryan et al. 2002) due to the meridional transport linked to the propagation of TIWs (notice the wave like shape of the bloom in Figure 9.3c).

A2: Despite the two 8-day composites being at the same seasonal time period, large differences in both SST and the phytoplankton community composition in Figure 9.3c, f, i and l are related to the fact that week 1 was during a large La Niña event (July/August 1998) and week 2 during non- El Niño/La Niña conditions. The inter-decadal occurrence of the El Niño/La Niña phenomena appears to be related to these differences.

Studies in the equatorial Pacific have suggested that diatoms do not contribute more than 20% of phytoplankton biomass (Blanchot et al. 2001; Kobayashi and Takahashi 2002; Dandonneau et al. 2004). Assuming diatoms comprise the majority of the microphytoplankton in the Equatorial Pacific, this value compliments our estimates of microphytoplankton % chlorophyll-*a* in non- El Niño/La Niña conditions (week 2, Figure 9.3b). However, blooms of diatoms have been reported in this area (Bender and McPhaden 1990; Chavez et al. 1990; Archer et al. 1997), particularly under La Niña events (Chavez et al. 1999; Strutton and Chavez 2000; Ryan et al. 2002; Alvain et al. 2008). Under such conditions, and using the algorithm of Brewin et al. (2010b), microphytoplankton appear to contribute as much as 70% of the phytoplankton biomass (Figure 9.3a).

Iron limitation is especially important for diatoms (Boyd, 2002) and when nutrients and iron are abundant in the photic layer, diatoms grow rapidly and dominate the phytoplankton population. Using *in situ* measurements, Chavez et al. (1999) linked the elevated levels of macronutrients and enhanced supply of iron associated with the La Niña event, to an increase in the concentration of diatoms (Table 1, Chavez et al. 1999), supporting the results shown in Figure 9.3a-c.

Differences in nanophytoplankton between the two weeks are less pronounced with slight increases in nanophytoplankton % chlorophyll-*a* at the periphery of the microphytoplankton bloom in week 1 (Figure 9.3f). In contrast to microphytoplankton, picophytoplankton are seen to have much lower % chlorophyll-*a* across the equatorial Pacific in week 1 when compared with week 2 (Figure 9.3i).

A3: The higher SST values seen in the south-east equatorial Pacific during week 1 (Figure 9.3j and l) appear to correspond to changes in the composition of nano- and picophytoplankton. While much of this area is masked by cloud coverage in Figure

9.3c, f and i, there is a slightly higher % chlorophyll-*a* of picophytoplankton in week 1 when compared with week 2 (Figure 9.3i) in the south-east equatorial Pacific. The inverse is seen for nanophytoplankton (Figure 9.3f).

Since picophytoplankton are smaller in size, they have a higher surface-to-volume ratio than nanophytoplankton, and hence can absorb nutrients with high efficiency under nutrient limited conditions (Raven 1998). Therefore, in stratified, nutrient depleted areas, such as the southern Pacific subtropical gyre, picophytoplankton are expected to dominate (Chisholm 1992; Dandonneau et al. 2004; Ras et al. 2008).

When comparing Figure 9.3g with Figure 9.3h, the southern subtropical gyre (indexed by the high levels of picophytoplankton >60 % chlorophyll-*a* south of the equator) appears further north and east in Figure 9.3g when compared with Figure 9.3h, possibly causing these discrepancies. This may be linked to changes in physical forcing during a La Niña event.

9.7 Summary

In this example we have highlighted the strong link between the community composition of the phytoplankton in the equatorial Pacific and the inter-decadal physical forcing (in this case the El Niño/La Niña phenomena). Changes in the community structure of phytoplankton appear to reflect changes in temperature in the equatorial Pacific. Larger phytoplankton cell sizes are associated with dynamic systems where fresh nutrients are available, and smaller size classes are associated with stratified, nutrient depleted regions. This tight coupling between the biology and physics in the equatorial Pacific supports the idea that all the components of a system, physical, biological and chemical, are intertwined, and that each component of the system is intrinsically linked with another (Lovelock 1992).

Remote sensing makes it possible to collect data in dangerous or inaccessible areas. It can also compliment costly and slow data collection *in situ*, ensuring that areas or particles are not disturbed, and it offers repeat viewing and can be used to monitor wide areas synoptically, not possible by conventional ground sampling methods. However, the true capabilities of remote sensing can only come to fruition when it is used in conjunction with *in situ* based measurements, for calibration and validation purposes. With more optical and biological *in situ* measurements, quantitative development and validation of the satellite PFT algorithms can continue. Furthermore, the synergistic benefits of using these observational techniques in conjunction allow for well-constrained, accurate biological and geophysical parameters that can then be assimilated into mathematical models to improve their parameterisation and our understanding needed to predict future change.

9.8 Acknowledgements

The NASA SeaWiFS project team and the NASA Jet Propulsion Laboratory Physical Oceanography Distributed Active Archive Centre is acknowledged for satellite data and all contributors to the SeaBASS data set for *in situ* pigment data. This work is funded by the National Environmental Research Council, UK, the National Centre for Earth Observation and NERC Oceans 2025 programme (Themes 6 and 10).

9.9 References and further reading

Alvain S, Moulin C, Dandonneau Y, Breon FM (2005) Remote sensing of phytoplankton groups in case 1 waters from global SeaWiFS imagery. Deep-Sea Res I 52:1989-2004

Alvain S, Moulin C, Dandonneau Y, Loisel H (2008) Seasonal distribution and succession of dominant phytoplankton groups in the global ocean: A satellite view. Global Biogeochem Cycles 22:GB3001, doi:3010.1029/2007GB003154

Archer D, Aiken J, Balch W, Barber D, Dunne J, Flament P, Gardner W, Garside C, Goyet C, Johnson E, Kirchman D, McPhaden M, Newton J, Peltzer E, Welling L, White J, Yoder J (1997) A meeting place of great ocean currents: shipboard observations of a convergent front at 2 degrees N in the Pacific. Deep-Sea Res II 44:1827-1849

Behrenfeld MJ, Bale AJ, Kolber DD, Aiken J, Falkowski PG (1996) Confirmation of iron limitation of phytoplankton photosynthesis in the equatorial Pacific Ocean. Nature 383:508-511

Bender ML, McPhaden MJ (1990) Anomalous nutruent distribution in the equatorial Pacific in April 1988: Evidence for rapid biological uptake. Deep-Sea Res I 37:1075-1084

Blanchot J, Andre JM, Navarette C, Neveux J, Radenac MH (2001) Picophytoplankton in the equatorial Pacific: vertical distributions in the warm pool and in the high nutrient low chlorophyll conditions. Deep-Sea Res I 48:297-314

Boyd PW (2002) Environmental factors controlling phytoplankton processes in the Southern Ocean. J Phycol 38:844-861

Brewin RJW, Lavender SJ, Hardman-Mountford NJ, Hirata T, Raitsos DE, Barciela R (2008) An intercomparison of bio-optical techniques for detecting phytoplankton functional types from space Ocean Optics XIX. SPIE proceedings, PDF No. oo080577 (CDROM), Castelvecchio Pascoli, Italy, 6-10 Oct. 2008

Brewin RJW, Lavender SJ, Hardman-Mountford NJ, Hirata T (2010a) A spectral response approach for detecting dominant phytoplankton size class from satellite remote sensing. Acta Oceanol Sin 29:14-32

Brewin RJW, Sathyendranath S, Hirata T, Lavender SJ, Barciela R, Hardman-Mountford NJ (2010b) A three-component model of phytoplankton size class for the Atlantic Ocean. Ecol Model 221:1472-1483

Chavez FP, Buck KR, Barber RT (1990) Phytoplankton taxa in relation to primary production in the equatorial Pacific. Deep-Sea Res I 37:1733-1752

Chavez FP, Strutton PG, Friederich GE, Feely RA, Feldman GC, Foley DG, McPhaden MJ (1999) Biological and Chemical Response of the Equatorial Pacific Ocean to the 1997-98 El Niño. Science 286: 2126 - 2131

Chisholm SW (1992) Phytoplankton Size. In: Primary Productivity and Biogeochemical Cycles in the Sea edited by Falkowski PG, Woodhead AD pp 213-237, Springer, New York

Ciotti AM, Bricaud A (2006) Retrievals of a size parameter for phytoplankton and spectral light absorption by coloured detrital matter from water-leaving radiances at SeaWiFS channels in a continental shelf off Brazil. Limnol Oceanogr Methods 4:237-253

Coale KH, Fitzwater SE, Gordon RM, Johnson KS, Barber RT (1996) Control of community growth and export production by upwelled iron in the equatorial Pacific Ocean. Nature 379:621-624

Cullen JJ (1991) Hypotheses to explain high-nutrient conditions in the open sea. Limnol Oceanogr 36:1578-1599

Dandonneau Y, Deschamps PY, Nicolas JM, Loisel H, Blanchot J, Montel Y, Thieuleux F, Becu G (2004) Seasonal and interannual variability of ocean color and composition of phytoplankton communities in the North Atlantic, equatorial Pacific and South Pacific. Deep-Sea Res II 51:303-318

Devred E, Sathyendranath S, Stuart V, Maas H, Ulloa O, Platt T (2006) A two-component model of phytoplankton absorption in the open ocean: Theory and applications. J Geophys Res 111:C03011, dio:03010.01029/02005JC002880

Etcheto J, Boutin J, Dandonneau Y, Bakker DCE, Feely RA, Ling RD, Nightingale PD, Wanninkhof R (1999) Air-sea CO_2 flux variability in the equatorial Pacific Ocean near 110°W. Tellus 51B:734-747

Feely RA, Wanninkhof R, Takahashi T, Tans P (1999) Influence of El Nino on the Equatorial Pacific contribution to atmospheric CO2 accounts. Nature 398:597-601

Hansen B, Bjørnsen PK, Hansen PJ (1994) The size ratio between planktonic predators and their prey. Limnol Oceanogr 39:395-403

Hardman-Mountford NJ, Hirata T, Richardson KA, Aiken J (2008) An objective methodology for the classification of ecological pattern into biomes and provinces for the pelagic ocean. Remote Sens Environ 112:3341-3352

Hirata T, Aiken J, Hardman-Mountford NJ, Smyth TJ, Barlow RG (2008a) An absorption model to derive phytoplankton size classes from satellite ocean colour. Remote Sens Environ 112:3153-3159

Hirata T, Hardman-Mountford NJ, Aiken J, Smyth T, Barlow R, Martines-Vicente V, Fishwick J, Bernard S (2008b) Optical approach to derive phytoplankton size classes using ocean color remote sensing. Ocean Optics XIX, Castelvecchio Pascoli, Italy, 6-10 Oct. 2008

Hirata T, Hardman-Mountford NJ, Brewin, RJW, Aiken J, Barlow R, Suzuki K, Isada T, Howell E, Hashioka T, Noguchi-Aita M, Yamanaka Y (2010) Synoptic relationships quantified between surface Chlorophyll-a and diagnostic pigments specific to phytoplankton functional types. Biogeosciences Discuss 7:6675-6704

Jennings S, Warr KJ, Mackinson S (2002) Use of size-based production and stable isotope analyses to predict trophic transfer efficiencies and predator-prey body mass ratios in food webs. Mar Ecol Prog Ser 240:11-20

Kerr RA (1998) Models win big in forecasting El Niño. Science 280:522-523

Kobayashi F, Takahashi K (2002) Distribution of diatoms along the equatorial transect in the western and central Pacific during the 1999 La Nina conditions. Deep-Sea Res II 49:2801-2821

Kostadinov TS, Siegel DA, Maritorena S (2009) Retrieval of the particle size distribution from satellite ocean colour observations. J Geophys Res 114:C09015, dio:09010.01029/02009JC005303

Le Quéré C, Harrison SP, Prentice CI, Buitenhuis ET, Aumont O, Bopp L, Claustre H, Cotrim Da Cunha L, Geider R, Giraud X, Klaas C, Kohfeld KE, Legendre L, Manizza M, Platt T, Rivkin R, Sathyendranath S, Uitz J, Watson AJ, Wolf-Gladrow D (2005) Ecosystem dynamics based on plankton functional types for global ocean biogeochemistry models. Glob Change Biol 11:2016-2040

Lovelock JE (1992) A numerical model for biodiversity. Philos Trans R Soc B Bio Sci 338:383-391, doi: 310.1098/rstb.1992.0156

Martin JH, Fitzwater SE (1988) Iron deficiency limits phytoplankton growth in the north-east Pacific subarctic. Nature 331:341-343

Martin JH (1991) Iron, Liebig's Law, and the Greenhouse. Oceanography 4:52-55

McPhaden MJ (1999) Genesis and evolution of the 1997-98 El Niño. Science 283:950-954

Nair A, Sathyendranath S, Platt T, Morales J, Stuart V, Forget M-H, Devred E, Bouman H (2008) Remote sensing of phytoplankton functional types. Remote Sens Environ 112:3366-3375

Raitsos DE, Lavender SJ, Maravelias CD, Haralambous J, Richardson AJ, Reid PC (2008) Identifying four phytoplankton functional types from space: An ecological approach. Limnol Oceanogr 53(2):605-613

Ras J, Claustre H, Uitz J (2008) Spatial variability of phytoplankton pigment distributions in the Subtropical South Pacific Ocean: a comparsion between *in situ* and predicted data. Biogeosciences 5:353-369

Raven JA (1998) Small is beautiful: The picophytoplankton. Funct Ecol 12:503-513

Ryan JP, Polito PS, Strutton PG, Chavez FP (2002) Unusual large-scale phytoplankton blooms in the equatorial Pacific. Prog Oceanogr 55:263-285

Sathyendranath S, Stuart V, Cota G, Maas H, Platt T (2001) Remote sensing of phytoplankton pigments: a comparison of empirical and theoretical approaches. Int J Remote Sensing 22:249-273

Sathyendranath S, Watts L, Devred E, Platt T, Caverhill C, Maass H (2004) Discrimination of diatoms from other phytoplankton using ocean-colour data. Mar Ecol Prog Ser 272:59-68

Scharf FS, Juanes F, Rountree RA (2000) Predator size - prey size relationships of marine fish predators: interspecific variation and effects of ontogeny and body size on trophic-niche breadth. Mar Ecol Prog Ser 208:229-248

Strutton PG, Chavez FP (2000) Primary productivity in the equatorial Pacific during the 1997-1998 El Niño. J Geophys Res 105:26089-26101

Takahashi T, Sutherland SC, Sweeney C, Poisson A, Metzl N, Tilbrook B, Bates N, Wanninkhof R, Feely RA, Sabine C, Olafsson J, Nojiri Y (2002) Global sea-air CO_2 flux based on climatological surface ocean pCO_2 and seasonal biological and temperature effects. Deep-Sea Res II 49:1601-1622

Thomas WH (1979) Anomalous nutrient-chlorophyll interrelationships in the offshore eastern tropical Pacific Ocean. J Mar Res 37:327-335

Toggweiler JR, Carson S (1995) What are upwelling systems contributing to the ocean's carbon and nutrient budgets? In: Summerhayes CP, Emeis KC, Angel MV, Smith RL, Zeitzschel B (eds) Upwelling in the ocean. Modern processes and ancient records. John Wiley & Sons, Chichester, UK, p 337-360

Uitz J, Claustre H, Morel A, Hooker SB (2006) Vertical distribution of phytoplankton communities in open ocean: An assessment based on surface chlorophyll. J Geophys Res 111:CO8005, doi:8010.1029/2005JC003207

Vidussi F, Claustre H, Manca BB, Luchetta A, Marty JC (2001) Phytoplankton pigment distribution in relation to upper thermocline circulation in the eastern Mediterranean Sea during winter. J Geophys Res 106(C9):19,939-919,956

Walsh JJ (1976) Herbivory as a factor in patterns of nutrient utilization in sea. Limnol Oceanogr 21:1-13

Werdell PJ, Bailey SW (2002) The SeaWiFS Bio-optical Archive and Storage System (SeaBASS): Current architecture and implementation. NASA Tech. Memo. 2002-211617. In: Fargion GS, McClain C (eds) NASA Goddard Space Flight Center. Greenbelt, Maryland, 45 pp